ChemPubSoc Europe

DOI: 10.1002/cssc.201501518

CHEMSUSCHEM Full Papers

Synthesis of C_4 and C_8 Chemicals from Ethanol on MgO-Incorporated Faujasite Catalysts with Balanced Confinement Effects and Basicity

Lu Zhang,[a] Tu N. Pham,[a] Jimmy Faria,[b] Daniel Santhanaraj,[a] Tawan Sooknoi,[a] Qiaohua Tan,[a] Zheng Zhao,[a] and Daniel E. Resasco*[a]

A new type of catalyst has been designed to adjust the basicity and level of molecular confinement of KNaX faujasites by controlled incorporation of Mg through ion exchange and precipitation of extraframework MgO clusters at varying loadings. The catalytic performance of these catalysts was compared in the conversion of C_2 and C_4 aldehydes to value-added products. The product distribution depends on both the level of acetaldehyde conversion and the fraction of magnesium as extraframework species. These species form rather uniform and highly dispersed nanostructures that resemble nanopetals. Specifically, the sample containing Mg only in the form of exchangeable Mg^{2+} ions has much lower activity than those in which a significant fraction of Mg exists as extraframework MgO. Both the $(C_6+C_8)/C_4$ and C_8/C_6 ratios increase with additional extraframework Mg at high acetaldehyde conversion levels. These differences in product distribution can be attributed to 1) higher basicity density on the samples with extraframework species, and 2) enhanced confinement inside the zeolite cages in the presence of these species. Additionally, the formation of linear or aromatic C_8 aldehyde compounds depends on the position on the crotonaldehyde molecule from which abstraction of a proton occurs. In addition, catalysts with different confinement effects result in different C_8 products.

Introduction

Although biorefineries can produce bioethanol on a large scale,[1] the low return on investment, which is characteristic of commodities, challenges their economic profitability and ultimately the widespread use of bioethanol as a transportation fuel. Therefore, chemical conversion of bioethanol into more valuable commodity chemicals is a highly desirable option for its utilization.[2] The integration of energy and chemical production in biorefineries by combining existing fermentation facilities and chemical industrial production seems to be a crucial aspect in the development of the technology.[3]

For example, the conversion of ethanol to crotonaldehyde is a reaction that has been investigated extensively.[4–8] Crotonaldehyde is a highly reactive α,β-unsaturated aldehyde that can be used to produce the industrially valuable crotyl alcohol through chemoselective hydrogenation.[3] The two main steps in the conversion of ethanol into crotonaldehyde include dehydrogenation to acetaldehyde and aldol condensation to the C_4 product. The latter step is conducted on either acid or basic catalysts.[9–20] One of the key requirements of these catalysts is their selectivity to C_4 products to minimize excessive condensation to $\geq C_6$ products. In this scenario, zeolites appear to be potentially attractive catalysts to maximize the desirable product due to their enhanced shape and size selectivity. Adjustable molecular confinement when using zeolites as catalysts is a unique tool offered by zeolites to enhance selectivity. Previously, we investigated the aldol condensation of acetaldehyde over faujasite zeolites with varying silicon/aluminum ratios and different types of alkali-metal cations.[21] We found that the $C_4/(C_6+C_8)$ product ratio depended on a variety of factors, such as strength, density, and accessibility of basic sites. It was also shown that base-catalyzed condensation (C_4 and $\geq C_6$ products) dominated at temperatures around 230 °C, whereas acid-catalyzed acetalization prevailed below 180 °C. Because high reaction temperatures may lead to side products and faster deactivation, we investigate herein the modification of faujasite zeolites to improve their activity at low temperatures.

Due to its high basicity, MgO is an effective basic catalyst for aldol condensation, but, in general, it tends to generate excessive over-condensation products. For instance, acetaldehyde on MgO results in low $C_4/(C_6+C_8)$ product ratios as the conversion increases. Therefore, herein, we have investigated novel compositions of MgO-modified faujasites, which exhibit the desirable combination of the required basic properties of MgO for the aldol reaction with the confinement benefits of the faujasite zeolites, which inhibit excessive condensation. This work is motivated by numerous previous investigations that have demonstrated the incorporation of metal or metal oxide clusters inside zeolite cavities.[22–32] Herein, we have used several

[a] Dr. L. Zhang, Dr. T. N. Pham, Dr. D. Santhanaraj, Prof. T. Sooknoi, Dr. Q. Tan, Z. Zhao, Prof. D. E. Resasco
School of Chemical, Biological, and Materials Engineering
University of Oklahoma, Norman, OK 73019 (USA)
E-mail: resasco@ou.edu

[b] Dr. J. Faria
Abengoa Research, C/Energía Solar no. 1
Palmas Altas, Seville 41014 (Spain)

Supporting Information for this article can be found under http://dx.doi.org/10.1002/cssc.201501518.

MgO-modified faujasites as catalysts in acetaldehyde/ethanol mixtures and characterized them with a variety of characterization techniques.

Previously,[21] we described how the silicon/aluminum ratio and type of alkali cation affected the selectivity to C_4 products. Herein, we additionally analyze how to tune the selectivity of different C_8 products when using the C_4 product crotonaldehyde as a feed. The C_8 products are mainly 2,4,6-octatrienal and tolualdehyde isomers. Both can have commercial interest. For instance, 2,4,6-octatrienal is a key intermediate for the synthesis of 2,4,6-octatrienoic acid and recent reports indicate that 2,4,6-octatrienoic acid is an effective UV radiation blocker that can be used in sunscreen products.[33] Likewise, tolualdehyde isomers are versatile starting materials for the synthesis of phthalic and terephthalic acids, which are used as intermediates in the production of phthalic anhydride and polyester polyethylene terephthalate (PET).[34] Only a few studies in the literature describe the synthesis of octatrienal and tolualdehyde by aldol condensation. We have found that excessive condensation to $>C_8$ products can be inhibited, if the corresponding C_8 alcohols are formed through the Meerwein–Pondorf–Verley (MPV) hydrogen-transfer reaction. Therefore, in this part of the study, isopropanol was chosen as the solvent because it was a better hydrogen donor than ethanol.

Results and Discussion

Table 1 shows the conditions used to incorporate MgO into the zeolite samples, as well as the contents of MgO in each zeolite. The concentration of Mg^{2+} in the solution was adjusted to obtain the desired amount of MgO, which was measured by inductively coupled plasma optical emission spectroscopy (ICP-OES), along with those of the other elements in the zeolite (Si, Al, K, Na). As a result, the nominal positive/negative charge ratio could be calculated as (K^+, Na^+, $2\,Mg^{2+}$)/Al to determine the fraction of Mg as exchangeable Mg^{2+} or MgO. Because this charge ratio should be unity, any number larger than 1.0 indicates that a fraction of Mg is in the form of excess MgO. For example, when using a 0.01 M solution of Mg^{2+}, the resulting charge ratio was 0.99, which indicated that in this sample (MgO-KNaX-0.99) it was possible that most of the Mg was in the form of exchangeable Mg^{2+} ions, with no excess MgO. In contrast, when the exchange solution was 0.1 M Mg^{2+}, the resulting nominal charge ratio was 1.14, which indicated the presence of extraframework MgO in the sample (MgO-KNaX-1.14). Likewise, when a 1 M solution of Mg^{2+} was used in the ion-exchange procedure, the nominal charge ratio further increased to 1.32; an indication of a larger amount of excess MgO in this sample (MgO-KNaX-1.32). These numbers might slightly deviate if some of the exchanged Mg ions are in the form of $Mg(OH)^+$. However, because the sample is calcined after the incorporation of Mg, any Mg in the form of hydroxides ($Mg(OH)^+$ or $Mg(OH)_2$) is probably converted into Mg^{2+} or MgO.

Characterization of zeolites MgO-KNaX

SEM images of the KNaX and MgO-KNaX series of zeolites are shown in Figure 1. As expected from the charge analysis described above, the MgO-KNaX-0.99 sample with no excess MgO shows an overall surface morphology similar to that of KNaX, which exhibits only a somewhat rougher external surface than that of the parent zeolite. As shown below, XRD and NMR spectroscopy results indicate that the zeolite structure of this sample (MgO-KNaX-0.99) remains almost intact. In contrast, the MgO-KNaX-1.14 sample, with excess MgO, appears very different (Figure 1c). The surface of the sample is covered

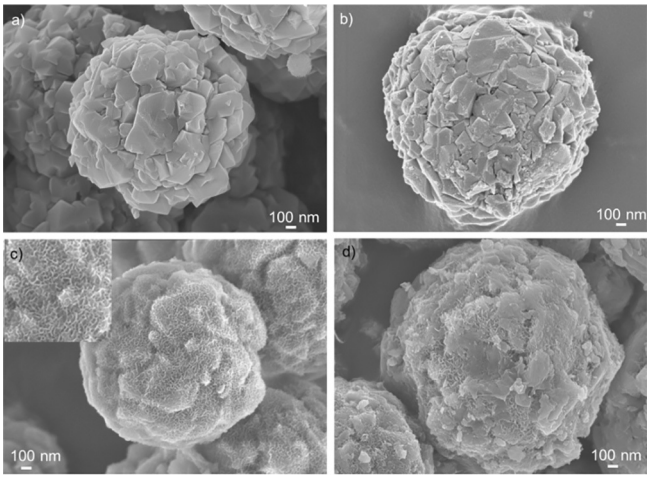

Figure 1. SEM images of a) KNaX, b) MgO-KNaX-0.99, c) MgO-KNaX-1.14, and d) MgO-KNaX-1.32.

Table 1. Preparation and resulting composition of MgO-incorporated zeolite catalysts.

Catalyst[a]	Concentration of Mg^{2+} for ion exchange (M)	Alkaline wash	Mg [wt%]	Si/Al	K^+/Na^+	Mg^{2+}/Na^+	(K^+, Na^+)/Al	(K^+, Na^+, $2\,Mg^{2+}$)/Al
KNaX	N/A[b]	N/A[b]	0.0	1.09	0.32	0.0	0.99	0.99
MgO-KNaX-0.99	0.01	KOH	1.3	1.09	0.49	0.21	0.72	0.99
MgO-KNaX-1.14	0.10	KOH	3.1	1.06	1.40	0.96	0.64	1.14
1st cycle catalyst[c]	N/A[b]	N/A[b]	3.6	1.04	1.22	0.74	0.66	1.10
2nd cycle catalyst[d]	N/A[b]	N/A[b]	3.6	1.03	1.17	0.72	0.67	1.10
MgO-KNaX-1.32	1.0	KOH	4.2	1.02	31.5	17.4	0.64	1.32

[a] The name code of the MgO-incorporated zeolite catalysts is based on the total positive to negative charge ratio indicated in the last column. [b] N/A = not applicable. [c] The first cycle catalyst was obtained by washing the used MgO-KNaX-1.14 catalyst with acetone followed by drying in an oven. [d] The second cycle catalyst was obtained by washing the used first cycle catalyst after the second cycle test with acetone followed by drying in an oven.

by a high density of nanostructures, which resemble nanopetals, as recently named by Koh et al.[35] Similarly, the MgO-KNaX-1.32 sample with even higher excess MgO also has a high density of nanopetals, but this sample also exhibits other plate-like structures (Figure 1 d). As shown below, this is an indication of MgO nanoparticles coating the surface.

The XRD patterns and NMR spectra were obtained to examine structural changes of the zeolite framework. The results are illustrated in Figures 2 and 3 (see below), respectively. As shown in Figure 2, only diffraction peaks due to the faujasite

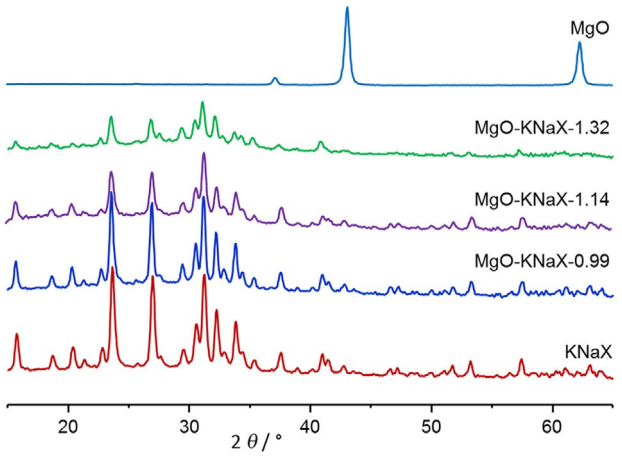

Figure 2. XRD patterns of zeolite samples and commercial MgO.

zeolite are observed for all MgO-KNaX samples, with no diffraction peaks that could be ascribed to MgO. This result suggests that the MgO particles are either too small in size or in concentration to be detected by XRD, which is expected. As shown in Table 1, none of the three MgO-modified samples contain more than 4 wt% of Mg. The ^{27}Al and ^{29}Si spectra for MgO-KNaX-0.99 agree with those of KNaX reported in Ref. [36], which again demonstrates that MgO-KNaX-0.99 retains an unchanged zeolite structure. Interestingly, the intensity of all diffraction peaks decreased as the MgO content increased from 1.14 to 1.32.

The XRD intensity drop for the MgO-KNaX-1.14 is likely to be due to the presence of MgO nanopetals coating the zeolite, since no shift in the NMR signals or appearance of new signals was detected (Figure 3). Any structural collapse would generate a change in the octa-/tetrahedral signal ratio or at least a shift in the position of the signal. The sample with higher Mg content (MgO-KNaX-1.32) showed a slight shift of the tetrahedral ^{27}Al signal from $\delta = 62$ to 60 ppm, as well as the appearance of a new signal at $\delta = 9$ ppm, which could be assigned to amorphous alumina.[37] In parallel, the corresponding ^{29}Si NMR spectrum for the MgO-KNaX-1.32 sample showed a dominant signal at $\delta = -88$ ppm, instead of the strong one at $\delta = -85$ ppm coupled with a weak one at $\delta = -89$ ppm observed in the spectra of both MgO-KNaX-0.99 and −1.14. These two ^{29}Si signals ($\delta = -85$ and $-88/-89$ ppm) are due to $Si(OAl)_4$ and $Si(OAl)_3(OSi)_1$ species, respectively.[41] This behavior is in agreement with the changes observed in the ^{27}Al spectra and indicates a minor modification of the zeolite structure in the MgO-KNaX-1.32 sample due to the high concentration of the alkaline solution (1 M) used in the preparation of this sample. As observed in Table 1, the Si/Al ratio in MgO-KNaX-1.32 is 1.02, which is very close to the original value of 1.09 in the parent KNaX, which indicates that any structural modification by KOH is insignificant compared with those observed in conventional desilication treatments. Therefore, the intensity drop observed in the XRD pattern of this sample (Figure 2) is a result of two factors, namely, coating of the external surface by MgO nanostructures and structural modification during preparation. We describe our SEM/TEM/energy-dispersive X-ray spectroscopy (EDX) results for a sliced specimen of the MgO-KNaX-1.32 sample prepared by a focused ion beam (FIB) in the Supporting Information. This technique uses a fine FIB to create very precise cross sections of a sample for subsequent imaging by SEM and TEM. The FIB allows thin slices of the zeolite sample to be produced; these can be scanned in different zones to determine whether there is an accumulation of magnesium on the external surface of the crystallites. Although the resolution of EDX is not enough to probe the nature of magnesium species inside and outside the zeolite, it is clear that magnesium is in both the internal and external regions. Notably, in the synthetic procedure used, the original KNaX zeolite was first exchanged with Mg^{2+} ions. Because K^+ and Na^+ ions are located inside the supercages of the parent KNaX sample, the Mg^{2+} ions introduced by the ion-exchange method should also be inside the pores. In the subsequent step, a KOH wash is conducted to precipitate Mg^{2+} as $Mg(OH)_2$, which is then calcined to form MgO. At this point, nanopetals are formed on the external surface, as clearly shown by SEM. The FIB/SEM/EDX results show that the region of the external surface contains all cations (Mg, Si, and Al) and, although there are regions

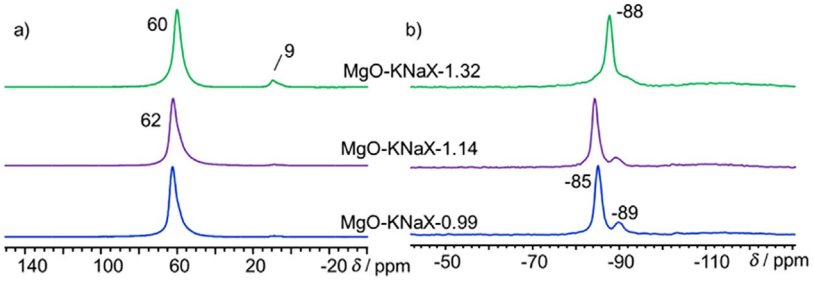

Figure 3. a) ^{27}Al and b) ^{29}Si MAS NMR spectra of zeolite samples.

that are enriched in Mg, it is not possible to determine whether the observed nanopetal features are made entirely of MgO or contain some Si or Al. Because Mg^{2+} ions were initially inside the pores, it is reasonable to believe that part of the MgO species are also located inside the pores.

The growth of $Mg(OH)_2$ nanostructures on zeolite A has been previously reported.[35,38] For example, Koh et al. found that the precipitation of petal-like nanostructures was controlled by the pH of the solution.[35] If the pH is above the isoelectric point of $Mg(OH)_2$, the $Mg(OH)_2$ nuclei are negatively charged and attract Na^+ ions to decrease the surface energy. Irregularly shaped nanoparticles are formed on the surface. On the other hand, with lower pH, $Mg(OH)_2$ nanopetals are observed. Herein, different morphology observed for the MgO-KNaX samples was controlled by the concentration of the solution of KOH.

The nitrogen adsorption–desorption isotherms and pore size distribution curves are shown in Figure S1 in the Supporting Information. The porosity characteristics of the zeolite samples are shown in Table 2. The values of the pore volumes for the parent KNaX zeolite demonstrate its microporous characteristics, along with the presence of a small extent of mesopores. In comparison, all three MgO-modified zeolite samples exhibit smaller V_{micro} values together with some enhanced mesoporosity in the 5–15 nm range. It is clear that the KOH washes conducted on these samples cause a small extent of framework dissolution and generation of mesopores. The presence of a larger number of K^+ ions would also account for the observed decrease in V_{micro} (see the K^+/Na^+ ratio in Table 1). Interestingly, MgO-KNaX-0.99 presents a similar V_{meso}/V_{micro} ratio to that of KNaX, whereas the V_{meso}/V_{micro} ratios in MgO-KNaX-1.14 or -1.32 are almost twice as large as that of KNaX. The difference is ascribed to the MgO nanostructures created on the surface of the Mg-modified samples. Similarly, Lydon et al. found an increased external surface area due to $Mg(OH)_2$ nanostructures extending out from the surface of zeolite A.[38]

Table 2. Porosity characteristics of the zeolite catalysts.

Catalyst	V_{micro} [$cm^3 g^{-1}$]	V_{meso} [$cm^3 g^{-1}$]	V_{meso}/V_{micro}
KNaX	0.288	0.049	0.170
MgO-KNaX-0.99	0.212	0.065	0.149
MgO-KNaX-1.14	0.217	0.068	0.313
1st cycle catalyst[a]	0.069	0.087	1.261
2nd cycle catalyst[b]	0.058	0.102	1.759
MgO-KNaX-1.32	0.237	0.072	0.378

[a] First cycle catalyst was obtained by washing the used MgO-KNaX-1.14 catalyst with acetone followed by drying in an oven. [b] Second cycle catalyst was obtained by washing the used first cycle catalyst after the second cycle test with acetone followed by drying in an oven.

The strength and density of basic sites were assessed by temperature programmed desorption (TPD) of adsorbed CO_2. As shown in Figure 4, the KNaX and MgO-KNaX-0.99 samples have similar TPD profiles, with a main desorption centered at about 100 °C. However, as the Mg loading increases, clear desorption peaks start emerging at higher temperatures. On MgO-KNaX-1.14, in addition to the low-temperature desorption peak described above, two new ones centered at about 250 and 325 °C become apparent. As the MgO loading increases for sample MgO-KNaX-1.32, these peaks become more prominent. They are clearly correlated with a higher basicity due to MgO incorporated into the sample. Based on the corresponding areas for this sample, the one centered at 100 °C represents 51% of the total desorbed CO_2. Pure MgO displayed two clear desorption peaks at temperatures above 350 °C, which suggested that the Mg-modified faujasites displayed moderate basicity that could be controlled by the Mg loading. This potential for tailoring the basic properties of the zeolite opens up interesting possibilities for base-catalyzed reactions.

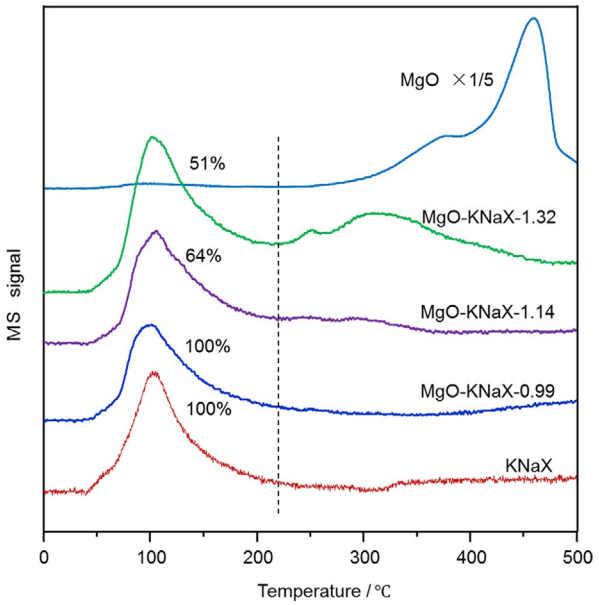

Figure 4. TPD profiles of CO_2 over zeolite catalysts and commercial MgO.

Production of C_4 compounds from acetaldehyde

Table 3 shows the catalytic performance of the different catalysts investigated for the reaction of acetaldehyde in ethanol. In all runs, the volume ratio of acetaldehyde/ethanol was kept at 1/10, by incorporating acetaldehyde (2 mL, 71.6 mmol of total C atoms) into ethanol (20 mL). The reaction was carried out at 180 °C for 3 h. As mentioned above, the activity of each sample was evaluated in terms of the amount of products obtained rather than the disappearance of acetaldehyde, which was highly volatile and could be additionally produced from the conversion of ethanol solvent. Because acid-catalyzed reactions are reversible, only condensation products are listed for comparison of activity.

Under the test conditions, only C_4 products formed over KNaX, but the total yields produced were only 1.5 mmol. At the other extreme, MgO with a higher strength and density basic sites, yielded about 48 mmol of condensation products. In this case, crotyl alcohol was the dominant product, as a result of a high MPV activity of MgO. However, the selectivity

Table 3. Total product yield and carbon selectivities from acetaldehyde/ethanol over zeolite and MgO catalysts.

Catalyst[a]	Product C yield [mmol]	C selectivities [%] crotonaldehyde + 3-hydroxybutanal	crotyl alcohol	butanal	butanol	mixed C_6	mixed C_8
KNaX	1.5	100	0.0	0.0	0.0	0.0	0.0
MgO-KNaX-0.99	9.2	94.5	0.0	0.0	5.5	0.0	0.0
MgO-KNaX-1.14	36.3	84.6	0.0	0.0	0.0	9.4	6.0
1st cycle catalyst[b]	23.3	89.9	0.5	0.0	0.0	4.9	4.7
physical mixture	40.6	70.3	0.6	0.0	1.1	15.3	12.7
MgO-KNaX-1.32	45.6	60.7	0.9	0.0	1.1	16.7	20.6
MgO	48.4	6.1	48.0	1.4	4.9	14.4	25.2

[a] Reaction conditions: batch reactor, 180 °C, 3 h reaction time, catalyst (400 mg), N_2 pressure 300 psi, stirring rate 300–400 rpm, solvent (ethanol)/reactant (acetaldehyde) volume ratio 10, acetaldehyde (2 mL). [b] First cycle catalyst was obtained by washing the used MgO-KNaX-1.14 catalyst with acetone followed by drying in an oven. The catalyst was then tested in a second reaction cycle to assess its stability.

to over-condensation ($\geq C_6$) products was also high. There was a low (1.4%) selectivity to butanol, which was produced from the C=C hydrogenation of crotyl alcohol. This reaction has been reported as a side reaction of MPV.[39] These results indicate that MgO is very active for combined aldol condensation and MPV reactions, but not selective to C_4 products.

As illustrated in Scheme 1,[21] the self-aldol condensation of acetaldehyde produces 3-hydroxybutanal, which readily dehydrates to form crotonaldehyde. Another well-known self-condensation pathway of acetaldehyde is the Tishchenko reaction, which gives ethyl acetate as a product.[40] Over-condensation can also occur to form $\geq C_6$ products. First, crotonaldehyde can self-condense to form C_8 products (2,4,6-octatrienal and tolualdehyde). It can also react with acetaldehyde to form C_6 products (2,4-hexadienal and 2-vinyl-crotonaldehyde). In turn, 2,4-hexadienal can react with acetaldehyde to form 2,4,6-octatrienal (C_8 product, by aldol condensation) or can undergo the Tishchenko esterification to form ethyl 3-hexenoate and ethyl hexanoate (C_8 products). In addition, the MPV reaction, which is catalyzed by Lewis acids or bases, is also a crucial reaction

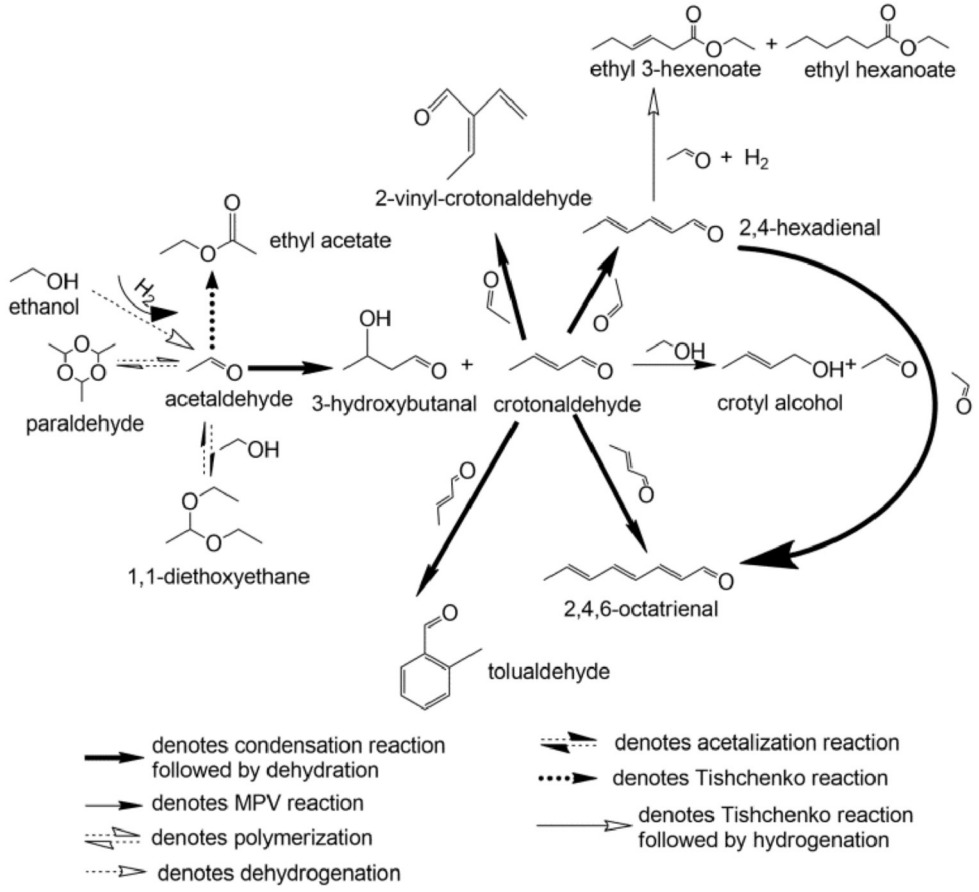

Scheme 1. Reaction network for aldol condensation of acetaldehyde in the liquid phase.

pathway that can be decisive in controlling the overall selectivity. In the presence of ethanol, crotonaldehyde can be reduced through the MPV reaction to form crotyl alcohol, while ethanol is oxidized to form acetaldehyde. Furthermore, acetaldehyde can oligomerize to form paraldehyde or form 1,1-diethoxyethane by the acid-catalyzed acetalization reaction. These two reactions are reversible. However, it either takes a longer reaction time or requires a higher reaction temperature for the products to return to acetaldehyde. The purpose of this work is to enhance the selectivity to the desired C_4 products at moderate conversion levels, which is typically low due to the many possible pathways. High selectivity to the C_4 products are usually only obtained at low conversions, under low reaction temperatures, and short reaction times.

Interesting differences and potential for selectivity optimization were observed on the MgO-incorporated faujasite samples. First, when Mg^{2+} was introduced in low concentrations into KNaX (sample MgO-KNaX-0.99 without excess MgO), the C_4 product yield increased about six times relative to that of KNaX, while the selectivity remained very high. With the presence of excess MgO the activity continued increasing. For instance, the MgO-KNaX-1.14 sample yielded about 20 times more products (36.3 mmol) than bare KNaX. It produced some C_6 and C_8 compounds, but the selectivity to C_4 products (84.6%) remained relatively high. Further increasing the MgO content, sample MgO-KNaX-1.32, improved the total yield by about 10 mmol compared with that for MgO-KNaX-1.14. However, this sample was much less selective, as indicated by a higher $\geq C_6$ product yield.

Figure 5 provides a comparison of the catalytic performances of the KNaX, MgO, and MgO-KNaX series. Under the same reaction conditions, the total condensation product yield increased with increasing MgO content. The MgO-KNaX-0.99 sample has all of the Mg in the exchangeable cation form (Table 1). The product yield from this sample was a fifth of the yield obtained over MgO. The MgO-KNaX-1.14 has 3 wt% Mg, with part of it in the form of extraframework MgO, and yielded almost the same amount of products as pure MgO. By further increasing the Mg content to about 4 wt% in the MgO-KNaX-1.32 sample, the performance became even closer to that of MgO. The result indicates that the incorporation of MgO into KNaX has indeed greatly enhanced the condensation activity. It is also demonstrated in Figure 5 that the undesirable $(C_6+C_8)/C_4$ product ratio increases with increasing MgO content, becoming a maximum on pure MgO. Therefore, it seems that an optimum can be found in terms of activity and selectivity at intermediate magnesium contents.

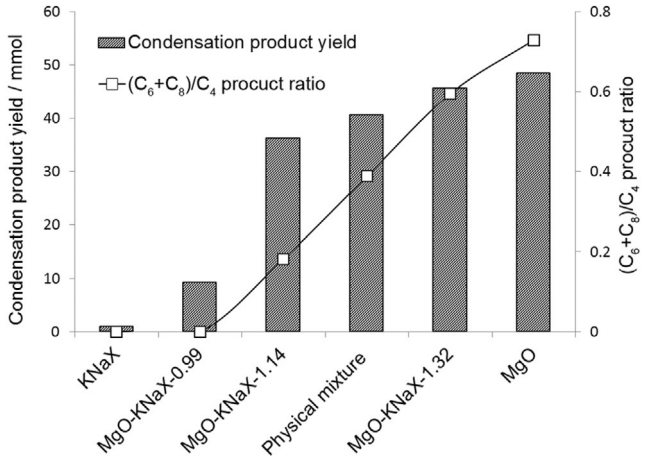

Figure 5. Product yield and distribution from acetaldehyde conversion at 180 °C over KNaX, MgO-incorporated zeolites, physical mixture of MgO and KNaX (3 wt% Mg), and MgO. Batch reactor at 180 °C, reaction time 3 h, catalyst weight 400 mg, N_2 pressure 300 psi, stirring rate 300–400 rpm, solvent (ethanol)/reactant (acetaldehyde) volume ratio 10 with acetaldehyde (2 mL).

The uniqueness of the catalytic properties of the Mg-modified faujasites is further supported by the results obtained with physical mixtures of MgO and KNaX, keeping the same overall Mg loadings as those of the Mg-modified faujasites. For example, a mixture with 3 wt% Mg, which is the same as that of MgO-KNaX-1.14, results in less C_4 products and more $\geq C_6$ products than that of MgO-KNaX-1.14 (see Table 3 and Figure 5).

Because selectivity may change with the level of conversion, a second series of experiments was conducted at comparable overall yields by adjusting the reaction time. This comparison is summarized in Figure 6. Because MgO-KNaX-0.99 was the least active catalyst among the three MgO-incorporated zeolites, it took 24 h of reaction time to reach about 30 mmol of total products, whereas it took only 1 h over MgO-KNaX-1.14 and -1.32 to achieve the same yield. With such a long reaction time, the $(C_6+C_8)/C_4$ product ratio became exceedingly high. However, as shown for runs at overall yields of 42–48 mmol (excluding MgO-KNaX-0.99), with samples containing excess MgO, the $(C_6+C_8)/C_4$ ratio increased with increasing Mg loading due to enhanced basicity. The influence of the catalyst composition became more prominent during experiments to vary the C_6/C_8 product ratio, which decreased with increasing loading of MgO in the catalyst; a trend that was more clearly defined at high conversion levels (see Figure 6b).

As proposed in our previous study,[21] the observed differences in $(C_6+C_8)/C_4$ and C_6/C_8 product ratios can be explained in terms of the differences in the density and location of basic sites in the catalysts. In other words, as shown in Table 1, with increased MgO loading in the MgO-KNaX series, correspondingly higher K/Na ratios were used. Therefore, we should expect less free space inside the cages for condensation reactions. In this case, most of the basic sites outside the cages account for base-catalyzed reactions, particularly those involving the larger molecules. As a result, over-condensation of C_4 to C_6 and C_8 products is favored due to a reduction in the steric confinement effect. At the same time, samples with excess Mg have a higher density of MgO nanoparticles covering the surfaces of the KNaX crystals than those with less Mg, which causes an increase in the amount of strong basic sites. Both effects result in an enhanced rate of over-condensation, which is clearly observed for the case of the sample with higher Mg loading (MgO-KNaX-1.32).

To test the stability and deactivation of the catalyst, experiments were performed with the recycled MgO-KNaX-1.14 catalyst (first cycle catalyst). As shown in Table 3, the product C

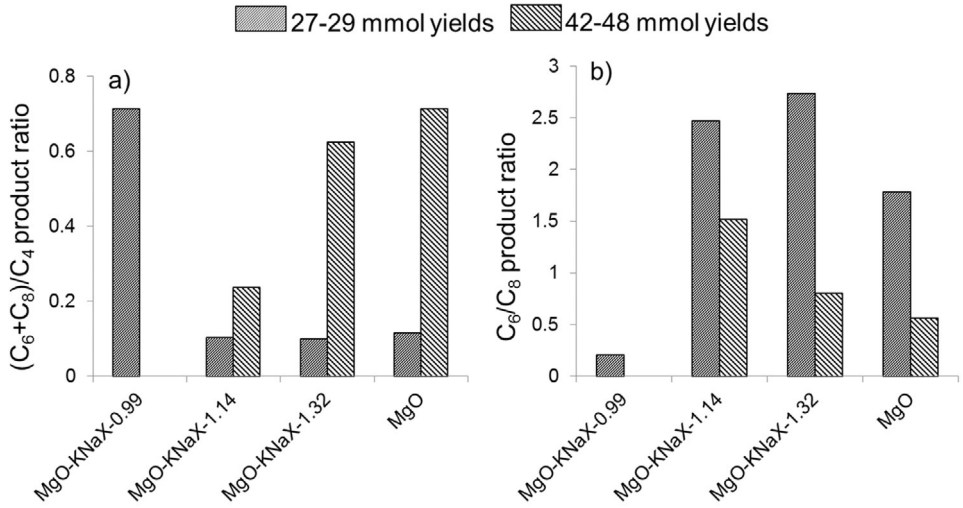

Figure 6. a) $(C_6+C_8)/C_4$ and b) C_6/C_8 product ratios from acetaldehyde conversion at 180 °C over MgO-incorporated zeolites and MgO. Batch reactor at 180 °C, N_2 pressure 300 psi, stirring rate 300–400 rpm, solvent (ethanol)/reactant (acetaldehyde) volume ratio 10 with acetaldehyde (2 mL).

yields decreased for the second cycle, but the C selectivities towards crotonaldehyde and 3-hydroxybutanal remained above 85% and almost 5% higher than over the fresh MgO-KNaX-1.14 catalyst. The C selectivities towards C_6 and C_8 products were also lower in the second cycle. The compositions and porosity characteristics, which are illustrated in Tables 1 and 2, show that the first cycle catalyst has a lower (K^+, Na^+, $2\,Mg^{2+}$)/Al ratio and much lower V_{micro} value than that of the fresh catalyst. Slight catalyst leaching and blockages of micropores due to large hydrocarbon molecules in the first cycle could explain differences in the recycle test results. Interestingly, the SEM image (Figure S2a in the Supporting Information) shows that the catalyst retained the nanopetal structures on the surface after the first reaction cycle. These results indicate that the observed differences could result from a decreased number of active sites in the microporous zeolite structure and those on the external surface. Additionally, despite significant structural changes after the first cycle test, the structure of the second cycle catalyst is similar to that of the first cycle (see Tables 1 and 2 and Figure S2 in the Supporting Information). Such observations suggest the high stability of the MgO-KNaX-1.14 catalyst in the second cycle test and beyond.

Synthesis of C_8 compounds

As mentioned earlier, 2,4,6-octatrienal and tolualdehyde are important intermediates for the synthesis of more valuable chemicals. They are also the main C_8 compounds produced in the aldol condensation of acetaldehyde in ethanol. As part of this study, crotonaldehyde was used as a reactant for the synthesis of C_8 molecules. To enhance the production of C_8, isopropanol was used as the solvent instead of ethanol because it was a better hydrogen donor for the MPV reaction, and limited the formation of heavy hydrocarbons by converting the C_8 aldehydes into alcohols and preventing the condensation reaction.

Scheme 2 illustrates the possible reaction network of crotonaldehyde conversion. The primary products 2,4,6-octatrienal and tolualdehyde are produced from the self-condensation of crotonaldehyde. The side reaction of C=C hydrogenation of crotonaldehyde produces butanal, whereas crotyl alcohol and acetone are produced from the MPV reaction of crotonaldehyde and isopropanol. Benzaldehyde can be formed through cross-aldol condensation between acetone produced and crotonaldehyde. In the presence of isopropanol, these condensation aldehydes undergo the MPV reaction to form their corresponding alcohols (2,4,6-octatrienol, tolyl alcohol, butanol, and benzyl alcohol). Additionally, butanol is also formed by the hydrogenation at the C=C bond of crotyl alcohol. Other possible products include 3-hydroxybutanal, which is a hydrated precursor of crotonaldehyde, and 3-buten-1-ol from the isomerization of crotyl alcohol.

In isopropanol, the MPV reaction may compete with self-condensation of the aldehydes. If the MPV reaction is exceedingly fast, crotonaldehyde may become crotyl alcohol before condensation, which is undesirable. On the other hand, if the MPV reaction is too slow, the C_8 aldehydes may continue condensing, which lowers the selectivity and causes catalyst deactivation. Because these two reactions can have different activation energies, one can vary the temperature to find conditions that maximize the yield of C_8 compounds. As an example, MgO was tested at four different temperatures, while keeping the other reaction parameters constant. As indicated in Table 4, at temperatures above 220 °C, the dominating product was crotyl alcohol, resulting from the MPV reaction. 3-Buten-1-ol was also formed, but in trace amounts. In contrast, at lower temperatures, octatrienal became the most abundant product. It is clear that the activation energy for the MPV reaction is higher than that for aldol condensation. However, at lower temperatures the overall yield decreases. As a result, as illustrated in Figure 7, the highest yield of C_8 products can be obtained at intermediate temperatures (≈180 °C). A much higher selectivity to tolualdehyde was also achieved at temperatures

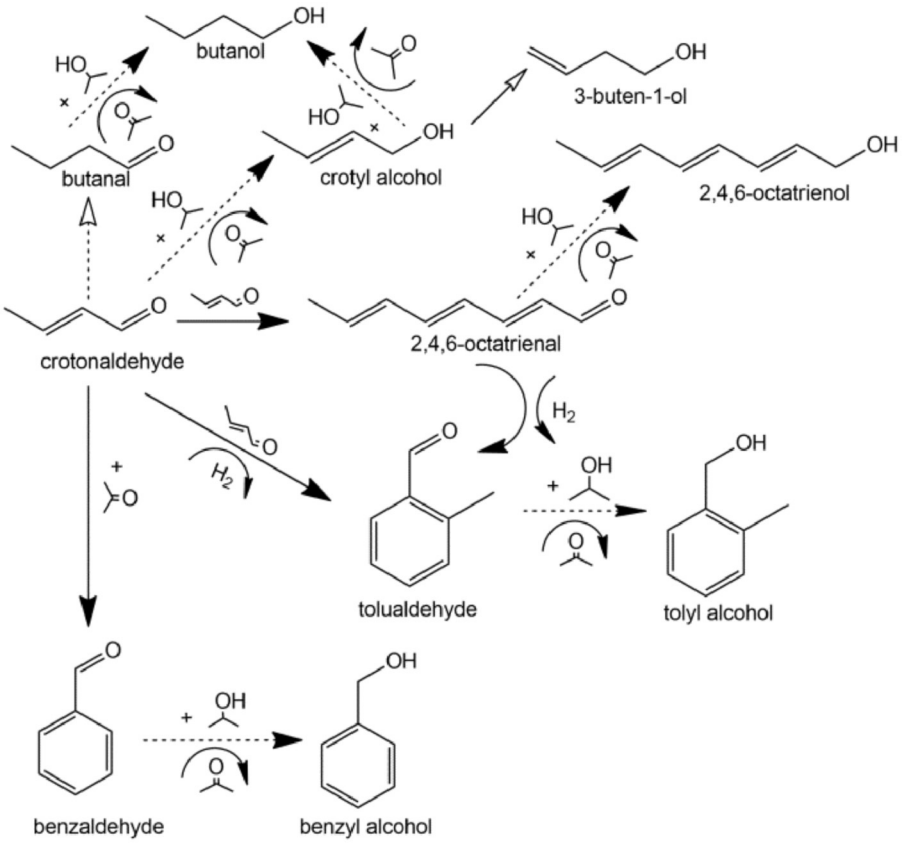

Scheme 2. Reaction network for the condensation of crotonaldehyde in the liquid phase.

Table 4. Conversion of crotonaldehyde as a function of temperature over MgO catalyst and product distribution.[a]

Temperature [°C]	Conversion [%]	Selectivity [%]				
		C_4OL	C_8	butanal + butanol	3-hydroxy-butanal	others
150	27.9	6.0	60.6	0.0	30.6	2.8
180	46.7	11.2	73.9	0.0	11.1	3.8
220	63.0	56.6	36.0	0.0	4.5	2.9
250	96.6	81.2	6.7	8.2	0.0	3.9

[a] C_4OL, includes crotyl alcohol and 3-buten-1-ol; C_8 includes octatrienal and tolualdehyde. Reaction conditions are the same as those given in Table 3.

below 180 °C. Because the C_8 condensation products were the target compounds, 180 °C was chosen as the reaction temperature for the comparison of the other catalysts.

Figure 8 a and b shows the octatrienal/tolualdehyde and *p*-/*o*-tolualdehye product ratios obtained at 180 °C over the different catalyst samples at low and high crotonaldehyde conversion levels. The selectivity trends for the magnesium faujasite catalysts is octatrienal > *p*-tolualdehyde > *o*-tolualdehyde and mostly independent of the conversion level. Interestingly, for KNaX and MgO-KNaX-0.99 (unmodified and slightly Mg-modified faujasite), the octatrienal/tolualdehyde and *p*-/*o*-tolualdehyde ratios are near one, whereas for the non-zeolitic basic catalysts (MgO and ZrO_2) these ratios are very high. Once

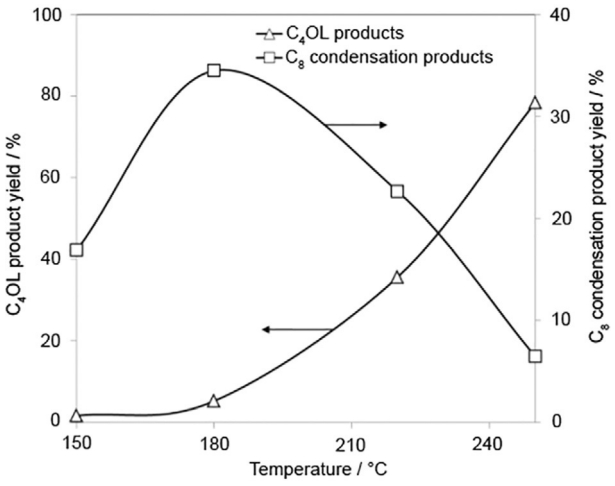

Figure 7. Conversion of crotonaldehyde as a function of temperature over MgO to compare the variation in yield to MPV C_4 products; C_4OL = crotyl alcohol + 3-buten-1-nol with that to condensation C_8 products. Catalyst weight 400 mg, N_2 pressure 300 psi, stirring rate 300–400 rpm, solvent (isopropanol)/reactant (crotonaldehyde) volume ratio 10 with crotonaldehyde (2 mL).

again the magnesium-modified faujasites show intermediate behavior between the two extremes.

Octatrienal is generated from the self-aldol condensation of crotonaldehyde. The base-catalyzed activation of crotonalde-

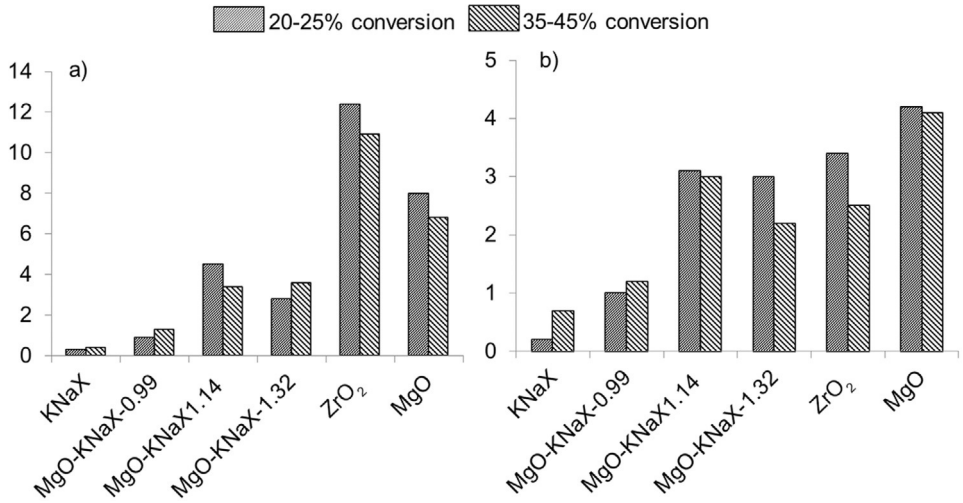

Figure 8. a) Octatrienal/tolualdehyde and b) *p*-/*o*-tolualdehye product selectivity ratios over zeolite catalysts, ZrO_2, and MgO at different conversion levels of crotonaldehyde. Batch reactor at 180 °C, N_2 pressure 300 psi, stirring rate 300–400 rpm, solvent (isopropanol)/reactant (crotonaldehyde) volume ratio 10 with crotonaldehyde (2 mL).

hyde, an α,β-unsaturated aldehyde, occurs at the vinylogous γ-C instead of the α-C, as typically occurs in aldehydes lacking the conjugated organic bonding system.[41] By attacking at the carbonyl group of another crotonaldehyde (1,2-addition), the resulting condensation product is the C_8 linear polyunsaturated aldehyde.[42] In contrast, if self-condensation of crotonaldehyde occurs through Michael addition (1,4-addition), both *o*- and *p*-tolualdehyde can be produced.[43] As shown in Scheme 3, this reaction entails the addition of a carbanion to the α-β unsaturated carbonyl compound. Both 1,2- and 1,4-addition of crotonaldehyde start with the formation of a carbanion intermediate by abstraction of a hydrogen atom from γ-C. The difference between the two pathways is that, after the common initial step, the carbanion undergoes nucleophilic addition to the carbonyl C of the second crotonaldehyde, yielding octatrienal (**4**), or to the β-C of the second crotonaldehyde, yielding tolualdehyde (**2**, **3**). Thus, the selectivity towards octatrienal versus tolualdehyde will depend on whether the carbonyl-C and β-C atoms of the crotonaldehyde facilitate the nucleophilic addition of the carbanion.

As shown in Table 5, the calculated distribution of charges on the C atoms of the crotonaldehyde molecule are about +1.62 around the carbonyl-C, which is much more positive than that of β-C (+0.10). Therefore, the higher electron deficiency of the former makes the aldol condensation path (1,2-addition) much more favorable than the Michael addition path (1,4-addition), which would involve the latter. This trend is in agreement with the experimental observation that, for most of the catalysts studied herein, the selectivity towards octatrienal (i.e., aldol condensation) is dominant. In contrast, the selectivi-

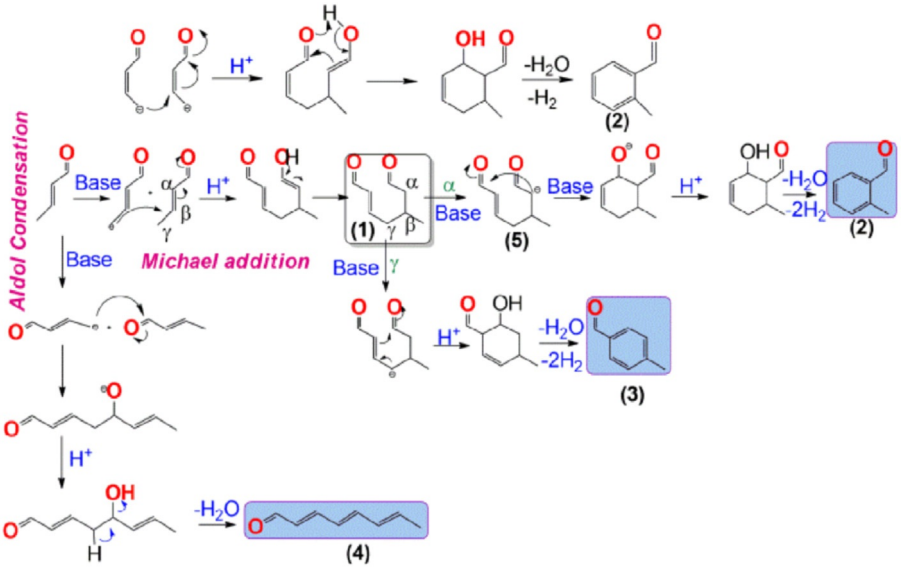

Scheme 3. Proposed reaction mechanism for the formation of C_8 compounds from crotonaldehyde.

Table 5. DFT-calculated charge distribution on the carbon atoms of crotonaldehyde.

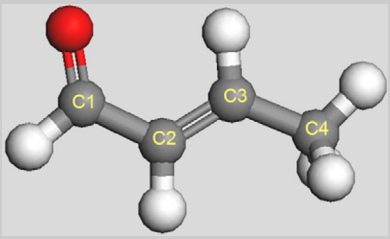

Carbon atom	Charge
C1	+1.62
C2	−0.12
C3	+0.10
C4	−0.04

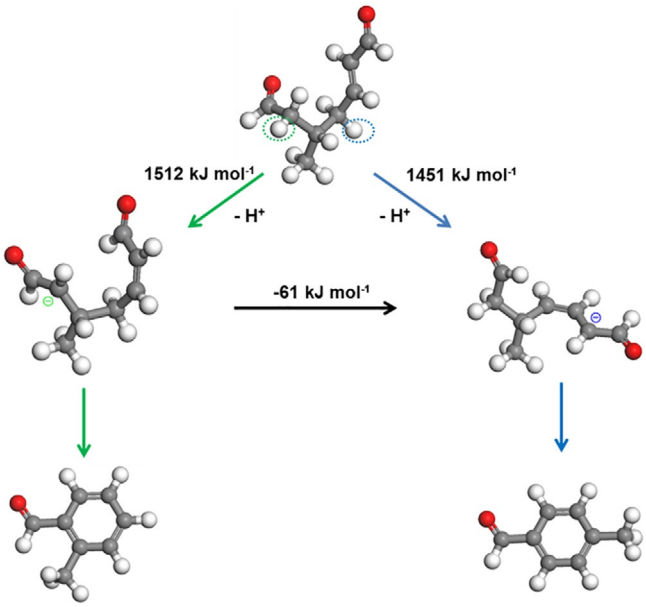

Figure 9. A summary of DFT-calculated gas-phase formation energies of the carbanion intermediates in the Michael addition reaction towards *o*- and *p*-tolualdehyde.

ty towards tolualdehyde (i.e., Michael addition) is only dominant for KNaX.

The first step of the Michael addition reaction of crotonaldehyde forms the intermediate 5-methyl-dihept-2-enal (**1**; Scheme 3), from which a hydrogen atom can be extracted from either the α or γ positions. Thus, two different carbanions can be formed, as shown in Scheme 3. Both of these carbanions can undergo nucleophilic addition to the carbonyl carbon atoms to form the ring intermediates, which finally lead to either *o*- (**2**; Scheme 3) or *p*-tolualdehyde (**3**; Scheme 3) through aromatization.[44] Thus, the selectivity towards *o*- or *p*-tolualdehyde is determined by the stability of the corresponding carbanion formed from the hydrogen abstraction of 5-methyl-dihept-2-enal at either the α or γ positions.

The formation energies of the two corresponding carbanions arising from hydrogen abstraction from 5-methyl-dihept-2-enal at either the α or γ positions were calculated (Figure 9). It is clear that the formation energy for the carbanion resulting from hydrogen abstraction at the γ position is about 60 kJ mol^{-1} lower than the formation energy of the carbanion obtained by removing one hydrogen at the α position. In other words, the path towards *p*-tolualdehyde has a lower energy barrier than that towards *o*-tolualdehyde, which is in agreement with the experimental observation that the selectivity to *p*-tolualdehyde is higher than that towards *o*-tolualdehyde on all catalysts, except those with lowest basicity, KNaX and MgO-KNaX-0.99.

An important question in interpreting the differences in selectivity observed herein among the different catalysts is whether the conversion of crotonaldehyde to octatrienal and tolualdehyde follows a parallel or sequential pathway. Is octatrienal the only primary product that subsequently cyclizes to form tolualdehyde or can tolualdehyde be formed directly from crotonaldehyde?

To address this question, the yield of each C_8 product was monitored as a function of reaction time over two catalysts: MgO-KNaX-1.32 and KNaX. Whereas the former shows a preference for octatrienal, the latter produces more tolualdehyde. As shown in Figure 10, even at the lowest conversion, MgO-KNaX-1.32 produces more octatrienal, whereas KNaX produces more

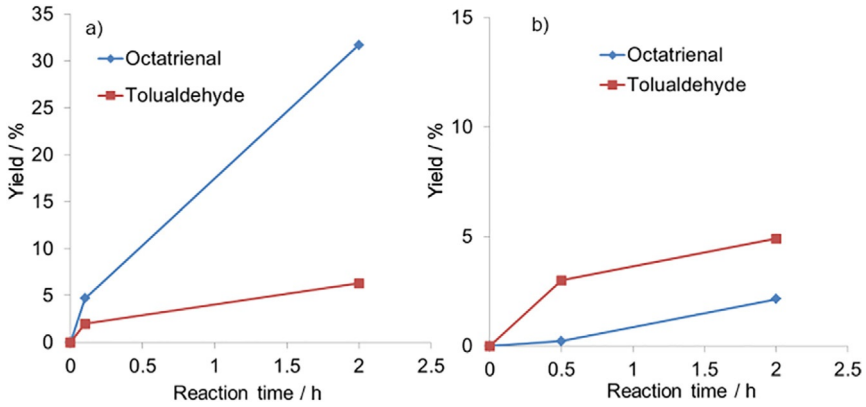

Figure 10. Yield of octatrienal and tolualdehyde for aldol condensation of crotonaldehyde over MgO-KNaX-1.32 (A) and KNaX (B) at 180 °C. Catalyst weight 400 mg, N_2 pressure 300 psi, stirring rate 300–400 rpm, solvent (isopropanol)/reactant (crotonaldehyde) volume ratio 10 with crotonaldehyde (2 mL).

tolualdehyde. Moreover, for the two catalysts, the yields of the two C_8 compounds increased simultaneously as the reaction time increased, and in both cases tolualdehyde seemed to be a primary product, which indicated that the formation of the two C_8 compounds followed parallel pathways with different initial selectivities, depending on the type of catalyst. There are two factors that can account for different product selectivities over KNaX and MgO-KNaX-0.99. One is basicity and the other is shape confinement in the pores. To resolve this issue, a ZrO_2 catalyst, with lower basicity than that of MgO and the absence of any confinement was tested under the same conditions. The catalytic results indicate that over ZrO_2 the octatrienal/tolualdehyde ratio was as high as, or even higher than, that of MgO (Figure 8A). This result suggests that the significantly lower octatrienal/tolualdehyde ratio observed over KNaX and MgO-KNaX-0.99 catalysts cannot be explained by a lower basicity, but rather mainly due to the confinement effect. One can propose that octatrienal may remain trapped inside the faujasite pores, whereas tolualdehyde may more easily diffuse out upon formation. Also, contrary to the other catalysts in the series, the two less-modified faujasite catalysts, KNaX and MgO-KNaX-0.99, exhibited a lower *p*-/*o*-tolualdehyde product ratio than the rest of the catalysts in the series. This could provide further evidence for the confinement effect of zeolites that facilitates ring closure without secondary proton abstraction, as proposed above (Scheme 3). Because these two samples contain higher Na^+ contents, this Lewis acid cation may effectively stabilize the enolate species, in a manner similar to that of the acid-catalyzed aldol condensation. One could expect that, after the first 1,4-addition, the α-carbon of 5-methyl-dihept-2-enal (enol form) would already be activated (see the Michael addition in Scheme 3). With the help of confinement and acidity derived from Na^+, the enol form of the adduct may subsequently undergo aldol condensation to the carbonyl at the other end before tautomerization to the aldehyde. This may lead to the formation of *o*-tolualdehyde without secondary deprotonation.

Conclusions

The basicity and extent of molecular confinement in KNaX zeolites have been adjusted by controlled incorporation of Mg as extraframework species through ion exchange and precipitation. The catalysts in the MgO-KNaX series exhibited significantly different performances for the extent of aldehyde condensation of C2 aldehyde, depending on the amount of extraframework MgO. Both the $(C_6+C_8)/C_4$ and C_8/C_6 ratios increased with increasing amounts of Mg outside the framework. Specifically, MgO-KNaX-0.99, which only has Mg in the cation form, is the least active condensation catalyst. MgO-KNaX-1.32 results in higher $(C_6+C_8)/C_4$ and C_8/C_6 ratios than those of MgO-KNaX-1.14, especially at high C2 aldehyde conversion levels. Differences in the product distribution are attributed not only to the higher basicity of MgO-KNaX-1.32, but also to the larger number of K^+ ions inside the supercages that increase the steric confinement and enhance conversion outside the zeolite cages. For instance, MgO-KNaX-1.32 has more heavily occupied supercages and higher density of basic sites on the surface. It thus favors over-condensation reactions to produce $\geq C_6$ and, in particular, C_8 products.

At the same time, molecular confinement seems to be the main factor that determines the selectivity towards linear or aromatic C_8 aldehyde products from the conversion of C_4 aldehyde. In other words, on the KNaX and MgO-KNaX zeolites containing Mg in the form of cations, the larger space available inside the cages favors ring closure and the formation of the aromatic C_8 aldehydes. In contrast, as the MgO loading increases, overcrowding of cations reduces the ring-closing ability of the catalyst and the favored C8 aldehyde product is linear octatrienal.

Experimental Section

Catalyst preparation

Magnesium oxide (MgO, $\geq$99%) was purchased from Sigma–Aldrich and used as received. Zirconium hydroxide purchased from Sigma–Aldrich was calcined at 500 °C for 3 h to form ZrO_2 before use. The parent faujasite KNaX zeolite (Si/Al = 1.0) was synthesized by a conventional hydrothermal method.[45] The MgO-modified faujasites were prepared as summarized in Scheme 4.[27] Mg^{2+} ions were introduced into the zeolite by the ion-exchange method, in which the zeolite sample (2 g) was contacted with an aqueous solution of $Mg(NO_3)_2$ (100 mL) at room temperature for 24 h. To adjust the content of Mg^{2+} ions in the zeolite, the concentration of the solution of $Mg(NO_3)_2$ was varied from 0.1 to 1 M. After filtration and drying overnight at 120 °C, the resulting Mg^{2+}-containing product was added to a solution of KOH (100 mL) to precipitate the Mg^{2+} ions in the $Mg(OH)_2$ form. In this step, the concentration of the alkaline solution was the same as that of the $Mg(NO_3)_2$ solution. After stirring for 20 min, the sample was recovered by filtration and washing with deionized water to reach a pH value close to 7. The solid sample obtained was then dried at 120 °C for 6 h, followed by calcination at 400 °C for 1 h, to obtain the MgO-modified faujasite product.

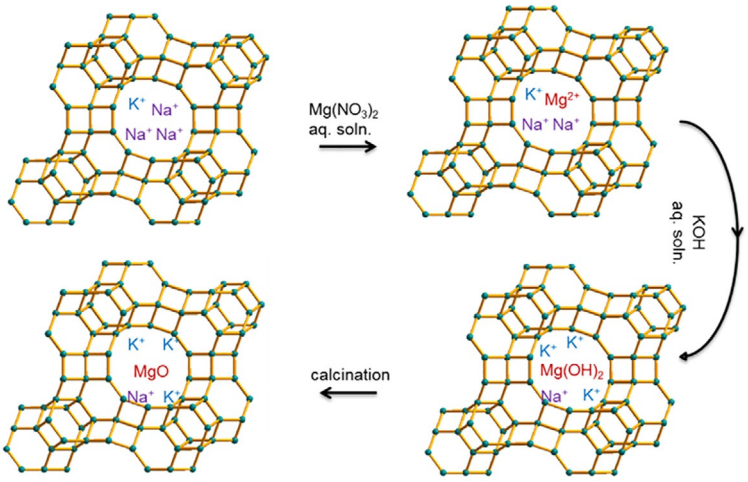

Scheme 4. Illustration of the incorporation of magnesium oxide into faujasite zeolite.

Catalyst characterization

Powder XRD patterns were recorded in reflection geometry on a D8 Series II X-ray diffractometer (Bruker AXS) that used $Cu_{K\alpha}$ radiation generated at 40 kV and 35 mA. The elemental compositions of all zeolite samples were determined by ICP-OES at Galbraith Laboratories.

^{27}Al and ^{29}Si NMR spectroscopy experiments were performed at Florida State University on a Bruker AVIII HD NMR spectrometer operating at a magnetic field strength of 11.74 T, equipped with a 4 mm Bruker MAS probe. For ^{27}Al MAS experiments, a single pulse acquisition was applied with a spinning speed of 14 kHz and a short RF pulse (less than 15°) with a recycle delay of 0.5–1 s. Spectra were collected after 10240 scans and referenced to $AlCl_3$ (aq. 1 M) at $\delta = 0$ ppm. For ^{29}Si MAS experiments, a single pulse acquisition (30° radiofrequency (RF) pulse) was applied with spinning rate of 12 kHz and a recycle delay of 25 s. Spectra were obtained after 4096 scans and referenced to tetrakis(trimethylsilyl)silane tetramethylsilane (TMSS) at $\delta = -10.2$ ppm.

The basicity of the catalysts was quantified by TPD of adsorbed CO_2.[30] Before chemisorption, a sample (200 mg) was heated in situ under a flow of He of 30 mL min^{-1} with a heating rate of 10 °C min^{-1} up to 200 °C, and held at this temperature for 3 h. After cooling the sample to room temperature, it was exposed to a 30 mL min^{-1} flow of CO_2 for 30 min and then it was purged with He for 2 h to remove physisorbed CO_2. TPD was performed under the same He flow rate by heating from 0 to 600 °C at a heating rate of 10 °C min^{-1}.

Catalytic reaction measurements

The aldol condensation of acetaldehyde was carried out in the liquid phase by using a high-pressure 50 mL stainless-steel autoclave batch reactor (Parr Corporation) equipped with impeller, temperature and pressure controllers, and sampling port. Ethanol was selected as the solvent to simulate conditions that might be encountered in a commercial process that used bioethanol as a feed to make acetaldehyde and a solvent. The reaction temperature was kept at 180 °C under a total pressure of 300 psi. In a typical experiment, a measured amount of catalyst was mixed with acetaldehyde and ethanol in the reactor vessel. After the reactor was sealed, it was purged with N_2 to 300 psi, and heated up to the desired reaction temperature with stirring at 300–400 rpm. In all runs, the initial ethanol/acetaldehyde volume ratio was kept at 10:1 (2 mL of acetaldehyde). After a given period of time, the reaction was quenched by rapid cooling. Liquid products were filtered and analyzed by using gas chromatography, GC-MS for product identification, and GC-FID for quantification. Chemical standards were used to obtain the retention times and response factors for all reactants and products.

Acetaldehyde was highly volatile at room temperature; therefore, it was difficult to prevent losses before analysis. Conversely, during the reaction, acetaldehyde was formed from the ethanol solvent through direct dehydrogenation or the MPV reaction. As a result, the amount of acetaldehyde remaining after the reaction was not a reliable measure of the extent of reaction to quantify precisely the catalytic activity of the different zeolite catalysts in a batch reactor. A more reliable measure of activity was the total moles of carbon in the products obtained during a given time period.

The self-condensation of crotonaldehyde to C_8 products was performed under similar conditions to those for acetaldehyde reaction, but with isopropanol as a solvent instead of ethanol. Here, the initial isopropanol/crotonaldehyde volume ratio was 10:1 (2 mL of crotonaldehyde). To quantify the activity, contrary to the case of the acetaldehyde/ethanol system, the conventional method of measuring conversion on the basis of reactant disappearance could be reliably applied because the C_8 compounds were not volatile and there was no conversion of the solvent into the reactant, as with the C_2 molecules. The selectivity in both cases was defined as the moles of carbon of a specific product to the total moles of carbon produced.

DFT calculations

Theoretical calculations were carried out by using gradient-corrected DFT methods implemented in DMol3.[46] Wave functions were represented by numerical basis sets of double numerical quality (DNP) with d-type polarization functions on each atom and expanded out to 3.5 Å cutoff. The Perdew–Wang 91 (PW91)[47] form of generalized gradient approximation (GGA) was used to model gradient corrections to correlation and exchange energies. The electronic density for each self-consistent iteration converged to within 10^{-5} au. The energy in each geometry optimization cycle was converged to within 2×10^{-5} Hartree within a maximum displacement and force of 4×10^{-3} Å and 3×10^{-3} Hartree $Å^{-1}$, respectively. Formation energies of carbanions were calculated as $RH \rightarrow R^- + H^+$, in which RH and R^- refer to the structure before removing one hydrogen and the carbanion formed. The distribution of charges was obtained by using the Bader charge analysis method.[48]

Acknowledgements

This research has been funded by Abengoa Research. Florida State University and U.S. NSF Major Research Instrumentation (MRI) program (NSF 1126587) are appreciated for the support of the solid-state NMR spectroscopic characterization.

Keywords: aldehydes · heterogeneous catalysis · magnesium · structure–activity relationships · zeolites

[1] H. van der Heijden, K. J. Ptasinski, *Energy* **2012**, *46*, 200 – 210.
[2] M. Balat, H. Balat, *Appl. Energy* **2009**, *86*, 2273 – 2282.
[3] J. J. Bozell, *Clean Soil Air Water* **2008**, *36*, 641 – 647.
[4] S. Kvisle, A. Aguero, R. Sneeden, *Appl. Catal.* **1988**, *43*, 117 – 131.
[5] S. Bhattacharyya, S. Sanyal, *J. Catal.* **1967**, *7*, 152 – 158.
[6] E. Makshina, W. Janssens, B. Sels, P. Jacobs, *Catal. Today* **2012**, *198*, 338 – 344.
[7] H. Jones, E. Stahly, B. Corson, *J. Am. Chem. Soc.* **1949**, *71*, 1822 – 1828.
[8] M. León, E. Díaz, S. Ordóñez, *Catal. Today* **2011**, *164*, 436 – 442.
[9] W. Ji, Y. Chen, H. H. Kung, *Appl. Catal. A* **1997**, *161*, 93 – 104.
[10] L. M. Baigrie, R. A. Cox, H. Slebocka-Tilk, M. Tencer, T. T. Tidwell, *J. Am. Chem. Soc.* **1985**, *107*, 3640 – 3645.
[11] R. N. Hayes, R. P. Grese, M. L. Gross, *J. Am. Chem. Soc.* **1989**, *111*, 8336 – 8341.
[12] O. Kikhtyanin, V. Kelbichová, D. Vitvarová, M. Kubů, D. Kubička, *Catal. Today* **2014**, *227*, 154 – 162.
[13] E. Dumitriu, V. Hulea, N. Bilba, G. Carja, A. Azzouz, *J. Mol. Catal.* **1993**, *79*, 175 – 185.
[14] Y.-C. Chang, A.-N. Ko, *Appl. Catal. A* **2000**, *190*, 149 – 155.
[15] E. Dumitriu, V. Hulea, I. Fechete, A. Auroux, J.-F. Lacaze, C. Guimon, *Microporous Mesoporous Mater.* **2001**, *43*, 341 – 359.
[16] S. Luo, J. L. Falconer, *Catal. Lett.* **1999**, *57*, 89 – 93.

[17] D. Tichit, D. Lutic, B. Coq, R. Durand, R. Reissier, *J. Catal.* **2003**, *219*, 167 – 175.
[18] B. Nozière, A. Córdova, *J. Phys. Chem. A* **2008**, *112*, 2827 – 2837.
[19] M. Singh, N. Zhou, D. K. Paul, K. J. Klabunde, *J. Catal.* **2008**, *260*, 371 – 379.
[20] J. E. Rekoske, M. A. Barteau, *Ind. Eng. Chem. Res.* **2011**, *50*, 41 – 51.
[21] L. Zhang, T. N. Pham, J. Faria, D. E. Resasco, *Appl. Catal. A* **2015**, *504*, 119 – 129.
[22] M. Zahmakıran, S. Özkar, *Appl. Catal. B* **2009**, *89*, 104 – 110.
[23] S. Kawi, J. Chang, B. Gates, *J. Am. Chem. Soc.* **1993**, *115*, 4830 – 4843.
[24] J. De Graaf, A. Van Dillen, K. De Jong, D. Koningsberger, *J. Catal.* **2001**, *203*, 307 – 321.
[25] B. Gates, *Chem. Rev.* **1995**, *95*, 511 – 522.
[26] W. M. Sachtler, *Acc. Chem. Res.* **1993**, *26*, 383 – 387.
[27] Q. Tang, Q. Zhang, P. Wang, Y. Wang, H. Wan, *Chem. Mater.* **2004**, *16*, 1967 – 1976.
[28] D. Fraenkel, B. C. Gates, *J. Am. Chem. Soc.* **1980**, *102*, 2478 – 2480.
[29] P. E. Hathaway, M. E. Davis, *J. Catal.* **1989**, *116*, 263 – 278.
[30] J. C. Kim, H.-X. Li, C.-Y. Chen, M. E. Davis, *Microporous Mater.* **1994**, *2*, 413 – 423.
[31] E. J. Doskocil, S. V. Bordawekar, B. G. Kaye, R. J. Davis, *J. Phys. Chem. B* **1999**, *103*, 6277 – 6282.
[32] R. J. Davis, E. J. Doskocil, S. Bordawekar, *Catal. Today* **2000**, *62*, 241 – 247.
[33] E. Flori, A. Mastrofrancesco, D. Kovacs, Y. Ramot, S. Briganti, B. Bellei, R. Paus, M. Picardo, *Pigm. Cell Melanoma Res.* **2011**, *24*, 618 – 630.
[34] T. Suzuki, A. Tateishi, S. Naito, (Mitsubishi Gas Chemical) US 4245078, **1981**.
[35] P.-Y. Koh, J. Yan, A. Teja, *J. Cryst. Growth* **2011**, *331*, 56 – 63.
[36] L. Zhang, Y. Huang, *J. Porous Mater.* **2015**, *22*, 843 – 850.
[37] E. Lippmaa, A. Samoson, M. Magi, *J. Am. Chem. Soc.* **1986**, *108*, 1730 – 1735.
[38] M. E. Lydon, K. A. Unocic, T.-H. Bae, C. W. Jones, S. Nair, *J. Phys. Chem. C* **2012**, *116*, 9636 – 9645.
[39] J. Mähler, I. Persson, *Inorg. Chem.* **2011**, *51*, 425 – 438.
[40] T. Seki, T. Nakajo, M. Onaka, *Chem. Lett.* **2006**, *35*, 824 – 829.
[41] R. C. Fuson, *Chem. Rev.* **1935**, *16*, 1 – 27.
[42] B. Campo, M. Volpe, S. Ivanova, R. Touroude, *J. Catal.* **2006**, *242*, 162 – 171.
[43] J. M. McIntosh, H. Khalil, D. W. Pillon, *J. Org. Chem.* **1980**, *45*, 3436 – 3439.
[44] P. Schiess, P. Fünfschilling, *Tetrahedron Lett.* **1972**, *51*, 5191 – 5194.
[45] G. H. Kühl, *Zeolites* **1987**, *7*, 451 – 457.
[46] MaterialStudio, V. 4.0, Accelyrys, Inc., San Diego, CA, **2010**.
[47] J. P. Perdew, J. Chevary, S. Vosko, K. A. Jackson, M. R. Pederson, D. Singh, C. Fiolhais, *Phys. Rev. B* **1992**, *46*, 6671 – 6687.
[48] W. Tang, E. Sanville, G. Henkelman, *J. Phys. Condens. Matter* **2009**, *21*, 084204.

Received: November 10, 2015
Published online on March 3, 2016